

Supplementary Information

High sensitivity indirect chemical detection using on-chip isotachopheresis with variable cross-section geometry

S.S. Bahga, G. V. Kaigala, M. Bercovici, and J.G. Santiago

Calculation of species concentrations in ITP zones using diffusion-free model

In Section 1.3 of the paper, we presented an unsteady, diffusion-free model to calculate species concentrations and shock speeds in ITP. We also showed (in Figure 2 of paper) comparison of our model with detailed 1-dimensional simulations using SPRESSO [1,2]. Here we describe the numerical procedure to calculate species concentrations in different ITP zones using our diffusion-free model. In Section 1.3 we derived Hugoniot jump conditions relating concentrations of each species across ITP shocks,

$$\frac{dx}{dt}(c_i^+ - c_i^-) = \frac{J}{A(x)} \left(\frac{\mu_i^+ c_i^+}{\sigma^+} - \frac{\mu_i^- c_i^-}{\sigma^-} \right), \quad \sigma = \sum_1^N z_i \mu_i c_i F. \quad (1)$$

where c_i , μ_i denote the concentration and effective mobility of species i , and σ denotes the electrical conductivity. Here J denotes the current, A the cross-sectional area and dx/dt the shock speed. In Eq. (1) – and + denote the evaluation of a property behind and in front of a shock, respectively.

Here we consider an ITP experiment with a leading electrolyte (LE), a trailing electrolyte (TE), an analyte (initially mixed with the TE) and a background electrolyte. In this case, two propagating shocks form corresponding to the adjusted-TE-to-analyte interface and the analyte-to-LE interface. Whereas the interface between the TE well and the adjusted TE zone remains stationary. See Zhukov [3] for more discussion on existence of propagating and stationary interfaces. The concentrations of species in the LE zone and the TE well are set by the initial conditions (when samples are loaded onto the chip). Whereas the species concentrations in the (plateau mode) analyte and the adjusted-TE zones matches the Jovin and Alberty functions [4,5] established by the LE. We therefore solve for the species concentrations in the analyte and the adjusted-TE zones.

First we solve for the species concentrations in the analyte zone by applying jump conditions (1) across the analyte-to-LE interface. Since analyte ions are not present in the LE zone (neglecting diffusion), the jump condition (1) for analyte concentration across the analyte-to-LE interface yields,

$$\frac{dx}{dt} c_{a,A} = \frac{J}{A(x)} \frac{\mu_{a,A}}{\sigma_A} c_{a,A}, \quad (1)$$

where σ_A denotes the conductivity of analyte zone, and $c_{a,A}$ and $\mu_{a,A}$ denote, respectively, the concentration and effective mobility of analyte in analyte zone. Recall that in our notation, the first small-case subscript identifies the ion, and the second capitalized subscript identifies the zone of interest. Similarly jump condition (1) for LE ions across the LE side of the analyte-to-LE interface gives,

$$\frac{dx}{dt} c_{l,L} = \frac{J}{A(x)} \frac{\mu_{l,L}}{\sigma_L} c_{l,L}, \quad (2)$$

From Eqs. (1) and (2) we obtain the speed of analyte-to-LE interface,

$$\frac{dx}{dt} = \frac{\mu_{a,A} J}{\sigma_A A} = \frac{\mu_{l,L} J}{\sigma_L A}. \quad (3)$$

The concentration of the background electrolyte (that is, the counter ion) in LE zone, $c_{b,L}$, is set by the initial conditions. Knowing $c_{b,L}$, we calculate the concentration of background electrolyte in the analyte zone, $c_{b,A}$, using jump condition (1) for background electrolyte across the analyte-to-LE interface,

$$\frac{dx}{dt}(c_{b,L} - c_{b,A}) = \frac{J}{A(x)} \left(\frac{\mu_{b,L}}{\sigma_L} c_{b,L} - \frac{\mu_{b,A}}{\sigma_A} c_{b,A} \right). \quad (4)$$

Substituting the value of dx/dt from Eq. (2) in Eq. (4), we obtain a simplified relation between concentrations of background electrolyte in the analyte and the LE zone,

$$\left(\frac{\mu_{i,L}}{\sigma_L} - \frac{\mu_{b,A}}{\sigma_A} \right) c_{b,A} = \left(\frac{\mu_{i,L}}{\sigma_L} - \frac{\mu_{b,L}}{\sigma_L} \right) c_{b,L}. \quad (5)$$

In the equations above, effective mobilities $\mu_{a,A}$ and $\mu_{b,A}$ depend on the pH of analyte zone. To calculate pH, we perform chemical equilibrium calculations based on the procedure described by Bercovici *et al.* [1]. In short, knowing the concentrations of analyte and background electrolyte we calculate the pH using acid-base equilibria and electroneutrality assumption. Equations (3) and (5), along with the electroneutrality assumption, form a set of three coupled non-linear algebraic equations in terms of $c_{a,A}$, $c_{b,A}$ and the pH of analyte zone. We solve this set of equations

numerically using *fsolve* routine of MATLAB to obtain the pH and the concentrations of analyte and background electrolyte in the analyte zone. We note that, for simplicity, we here neglected the effects of ionic strength on ion mobility and the acid-base equilibria. However, a process similar to that described above can be used to include these effects. See for example Bahga *et al.* [6] for a description of such a model. Also, Bahga *et al.* [6] showed that for univalent ions, calculated sample accumulation does not depend strongly on ionic strength effects on electrophoretic mobility.

Next, we solve for the remaining unknowns, namely the concentrations of analyte, TE and background electrolyte in the adjusted-TE zone. We apply jump conditions (1) across the adjusted-TE-to-analyte and the TE well-to-adjusted-TE interface to solve for the concentrations of analyte, TE and background electrolyte in the adjusted TE zone. Using the jump conditions (1) across the adjusted-TE-to-analyte interface (which moves at a speed of $\mu_{i,T}J/(\sigma_T A)$) we obtain,

$$\frac{\mu_{i,T}}{\sigma_T} (c_{b,A} - c_{b,T}) = \left(\frac{\mu_{b,A}}{\sigma_A} c_{b,A} - \frac{\mu_{b,T}}{\sigma_T} c_{b,T} \right), \quad (6)$$

$$\frac{\mu_{i,T}}{\sigma_T} (c_{a,A} - c_{a,T}) = \left(\frac{\mu_{a,A}}{\sigma_A} c_{a,A} - \frac{\mu_{a,T}}{\sigma_T} c_{a,T} \right). \quad (7)$$

Further, using the jump condition across the stationary interface between the TE well and the adjusted TE zone we obtain a relation between the concentration of TE in the adjusted-TE zone and the TE well,

$$\frac{\mu_{i,well}}{\sigma_{well}} c_{i,well} = \frac{\mu_{i,T}}{\sigma_T} c_{i,T}. \quad (8)$$

Here the species concentrations in the TE well are known from the initial conditions. Equations (6), (7) and (8) along with the electroneutrality assumption then form a set of four coupled algebraic equations in $c_{b,T}$, $c_{a,T}$, $c_{i,T}$ and the pH of adjusted-TE zone, which we solve numerically. Knowing the species concentrations in all ITP zones, we then evaluate the speeds of propagating interfaces.

Lastly, the analyte-to-LE interface propagates at a speed of $\mu_{i,L}J / (\sigma_L A) = \mu_{a,A}J / (\sigma_A A)$ while the adjusted-TE-to-analyte interface propagates at a speed of $\mu_{i,T}J / (\sigma_T A)$.

Dependence of SNR and assay time on channel geometry

In Section 2.2 of the paper, we showed that the plateau zone length of an analyte, Δ_p , is proportional to both the concentration of the analyte in the well, c_a^0 , and to the geometric parameter $A_L L_L / A_D$,

$$\Delta_p = \left(1 - \frac{\mu_{i,T}}{\mu_{a,T}} \right) \frac{\mu_a^0 \sigma_T}{\mu_{i,T} \sigma^0} \left(\frac{A_L L_L}{A_D} \right) \frac{c_a^0}{c_{a,A}}. \quad (9)$$

Recall that A_L and L_L are the cross-sectional area and length of the loading (larger cross-section) region of the channel, and A_D is the cross-sectional area of the detection (smaller cross-section) region. We see the theoretical plateau zone length is independent of the applied voltage or current. We here derive analytical relations for the dependence of SNR and assay time on channel geometry. SNR and assay time have different functional dependences for the cases of fixed current and fixed voltage. We therefore derive the analytical expressions for SNR and assay time separately for fixed voltage and fixed current operation.

Fixed Voltage

To estimate the assay time for fixed voltage operation, we calculate the time taken by the analyte zone to travel from the trailing electrolyte (TE) well to the detection section. Let x denote the coordinate of the interface between the analyte and leading electrolyte (LE). In the absence of electroosmotic flow (EOF), the speed of the analyte-to-LE interface in the loading section is given by

$$\frac{dx}{dt} = \frac{\mu_{i,L} J(x)}{A_L \sigma_L}, \quad (10)$$

where A_L is the cross-sectional area of the loading section, $\mu_{i,L}$ is the effective mobility of LE in the LE zone, σ_L is the conductivity of the LE zone and $J(x)$ is the current through the channel when the analyte-to-LE interface is at location x . We can approximately relate total current in the system to the applied voltage, ΔV , using Ohm's law,

$$\Delta V = JR, \quad R = \frac{x}{\sigma_T A_L} + \frac{L_L - x}{\sigma_L A_L} + \frac{L_D}{\sigma_L A_D}, \quad (11)$$

where σ_T is the conductivity of TE zone and A_D is the cross-sectional area of detection section. In Eq. (11) we have neglected the contribution of analyte zone to the electrical resistance of the channel. This is a reasonable approximation because the analyte zone length is much smaller than the LE and the TE zones. Also, within interfaces between zones, the diffusive current is non-negligible and so Ohm's law does not apply locally. However, we also assume these interfaces also contribute negligible resistance to the total axial-length-averaged resistance in the channel. Combining Eqs. (10) and (11) we obtain a differential equation relating time and the location of analyte-to-LE interface,

$$\frac{dt}{dx} = \frac{A_L}{\mu_{i,L}} \frac{\sigma_L}{\Delta V} \left(\frac{x}{\sigma_T A_L} + \frac{L_L - x}{\sigma_L A_L} + \frac{L_D}{\sigma_L A_D} \right). \quad (12)$$

To calculate the assay time, T , we integrate Eq. (12) up to $x = L_L$ (where the detection section begins)

$$T = \int_0^{L_L} \frac{A_L}{\mu_{i,L}} \frac{\sigma_L}{\Delta V} \left(\frac{x}{\sigma_T A_L} + \frac{L_L - x}{\sigma_L A_L} + \frac{L_D}{\sigma_L A_D} \right) dx. \quad (13)$$

Evaluating the integral above, we obtain an algebraic expression for the assay time for fixed voltage operation,

$$T = \frac{L_L L_D}{\mu_{i,L} \Delta V} \left(\frac{A_L}{A_D} + \frac{1}{2} \left(1 + \frac{\sigma_L}{\sigma_T} \right) \frac{L_L}{L_D} \right). \quad (14)$$

Next, we derive the dependence of SNR on geometric parameters. SNR is given by the length of the analyte plateau zone normalized by the characteristic length of diffused zone boundaries [7],

$$\text{SNR} = \frac{\Delta_p}{(\delta_{te,an} + \delta_{an,le}) / 2}. \quad (15)$$

Here $\delta_{te,an}$ and $\delta_{an,le}$ are, respectively, the characteristic widths of adjusted TE-to-analyte and analyte-to-LE interfaces in the detection section. For the characteristic width of an ITP interface, we use the analytical expression provided by Saville and Palusinski [8],

$$\delta_{1,2} = \frac{k_B T}{e} \frac{\mu_1 \sigma_2}{(\mu_2 - \mu_1) j}. \quad (16)$$

where subscripts 1 and 2 denote lower and higher mobility species corresponding to the zones adjoining a particular interface (e.g., for analyte-to-LE zone subscript 1 refers to the analyte and 2 refers to the LE). Here k_B is the Boltzmann constant, T the temperature, e the unit elementary charge and j ($= J / A_D$) the current density. To estimate the current, for Eq. (16), we substitute $x = L_L$ in Eq. (11). The corresponding current density is given by,

$$j = \frac{\Delta V \sigma_L}{L_D \left(1 + \frac{L_L A_D \sigma_L}{L_D A_L \sigma_T} \right)}. \quad (17)$$

This is the current density in the detector section, when the analyte-to-LE interface is at the junction of loading and detection section. Combining Eqs. (15), (16) and (17) we obtain the dependence of SNR on geometric parameters, A_L , A_D , L_L and L_D ,

$$\text{SNR} \propto \left(\frac{A_L L_L}{A_D L_D} \right) \left(1 + \frac{L_L A_D \sigma_L}{L_D A_L \sigma_T} \right)^{-1}. \quad (18)$$

Figure 1 shows the dependence of zone length (dashed contours) and interface thickness (solid line contours) on L_L and A_L / A_D , for fixed voltage. Here, we choose values of $L_D = 5$ mm and an applied potential of 350 V as typical values of interest. We note that smaller L_D values are often impractical as the channel can then become overly sensitive to pressure differences due to small differences in chip well liquid levels. From Eq. (9) zone length increases by increasing A_L / A_D and L_L . This is because, for larger cross-sectional area ratios and loading lengths, larger amounts of sample accumulates in the loading section. As a result, the zone length in the detection section increases. Additionally, Figure 1 shows that the interface thickness decreases by increasing

A_L / A_D and decreasing L_L . From Eq. (17), we see that current density in the detection section increases on increasing the cross-section ratio and decreasing loading length. Therefore the interface thickness, which is inversely proportional to current density, decreases by using higher cross-sectional area ratio and smaller loading length (since each of these increase electric field in the detector region).

Figure 2 shows the dependence of SNR (dashed contours) and assay time (solid line contours) on cross-sectional area ratio and the length of the loading section, for fixed voltage operation. SNR increases by increasing both the cross-section ratio and the length of loading section. On increasing A_L / A_D , the zone length increases (more accumulation) and the interface length decreases (more field in the detection region, as per Figure 1). Therefore SNR, which we define as the ratio of plateau zone length and characteristic interface thickness, increases for larger cross-sectional area ratios. However, for a fixed cross-section ratio, increasing the loading length increases both the zone length and the interface thickness. Hence in Figure 2, we observe a weak dependence of SNR on L_L , particularly at high A_L / A_D . Further, Figure 2 shows that, using larger cross-section ratio and loading length leads to longer assay time. For larger A_L / A_D , smaller voltage is dropped across the loading section. As a result, by increasing the cross-sectional area ratio, electric field in the loading section decreases. At lower electric field, ITP zones propagate slower and take longer time to reach the detection section, thereby increasing the assay time. Also, the assay time increases for longer loading section, as ITP zones have to travel a longer distance to reach the detection section.

For fixed voltage and SNR, increase in cross-sectional area ratio decreases the required channel length and also reduces the assay time. However, for a fixed loading length, larger cross-sectional area ratio yields higher SNR, but at the expense of longer assay time. Thus for a fixed voltage operation, there is a trade-off between SNR and assay time.

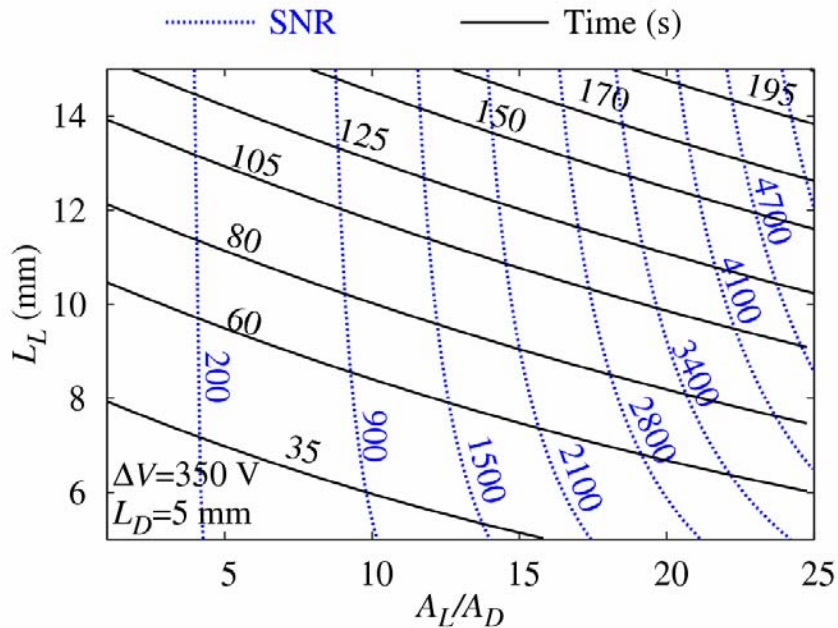


Figure 1: Effect of cross-sectional area ratio (A_L / A_D) and the length of loading section (L_L) on plateau zone length and interface thickness for fixed voltage operation. Dashed lines show contours of constant zone length for varying A_L / A_D and L_L . Zone length increases by increasing both,

A_L / A_D and L_L , since the amount of sample accumulated increases for larger A_L / A_D and L_L . Solid lines show the variation of diffusion-limited interface thickness (in the detection section) as a function of cross-section ratio and the length of loading section. Interface thickness decreases by increasing the cross-sectional area ratio and decreasing the loading length. For these calculations, we used a fixed voltage of 350 V and a detection section of length 5 mm. We calculated the values of conductivity of the LE and the adjusted TE zones, using our diffusion-free model, for ITP focusing of 2 μM Bistris (initially mixed with TE), with 10 mM NaOH as the LE, 10 mM Pyridine as the TE and 20 mM Hepes as the background counter-ion. The calculated conductivity of the LE zone is $7.28 \times 10^{-2} \text{ S.m}^{-1}$ and the conductivity of the adjusted TE zone is $4.7 \times 10^{-3} \text{ S.m}^{-1}$.

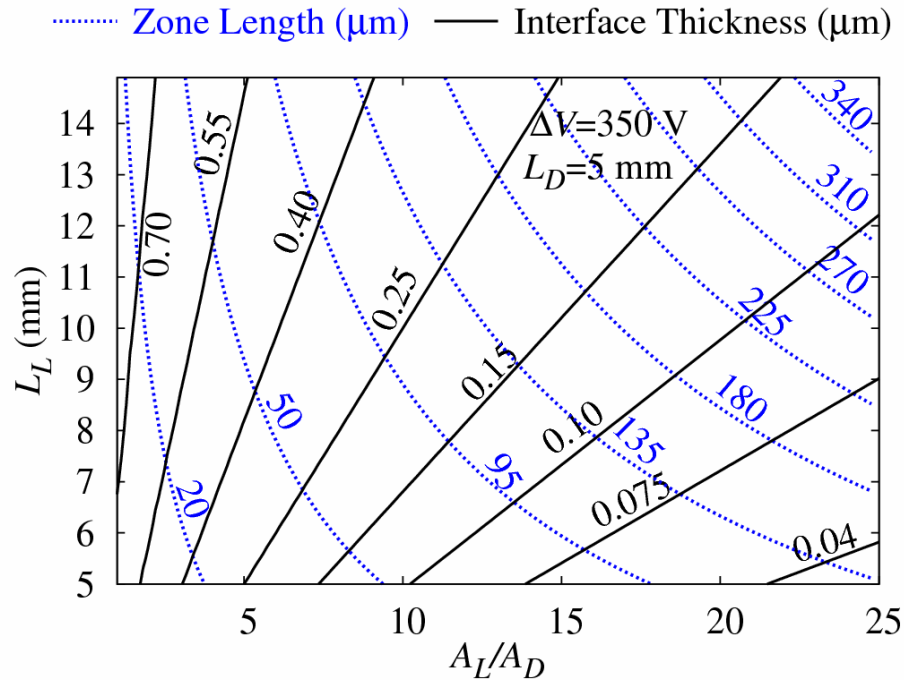


Figure 2: Effect of cross-sectional area ratio (A_L / A_D) and length of loading section (L_L) on signal-to-noise ratio (SNR) and assay time, for fixed voltage operation. Dotted lines show the variation of SNR as a function of A_L / A_D and L_L . SNR increases by increasing both the cross-sectional area ratio and the loading length. However, increasing A_L / A_D yields greater improvements in SNR as compared to that only increasing L_L . This is because increasing A_L / A_D results in longer zone length and sharper interfaces; while increasing L_L yields longer zone length but thicker zone boundaries. Solid lines show the contours of constant assay time for different cross-sectional area ratios and loading lengths. The assay time increases by increasing the cross-sectional area ratio as well as the loading length. Therefore, for fixed voltage operation, higher SNR can be achieved with the same physical length of channel but this is accompanied by longer assay time. All calculations here are based on the parameters used in Figure 1.

Fixed Current

We here estimate the dependence of assay time, interface thickness and SNR on channel geometry, for fixed current operation. To calculate the assay time, we integrate Eq. (10) to obtain an analytical expression for assay time.

$$T = \frac{\sigma_L A_L L_L}{\mu_{1,L} J}. \quad (19)$$

In this case, the calculation of assay time is straightforward because the current is fixed and the shocks move at constant speeds in the loading section. To obtain the interface thickness we substitute current density $j = J / A_D$ in Eq. (16) to obtain,

$$\delta_{1,2} = \frac{k_B T}{e} \frac{\mu_1 \sigma_2 A_D}{(\mu_2 - \mu_1) J}. \quad (20)$$

Using Eq. (15) and (20) we see that when fixed current is applied across a varying cross-section channel,

$$\text{SNR} \propto A_L L_L / A_D^2. \quad (21)$$

Figure 3, shows the contours of constant zone length, assay time and SNR for varying A_L / A_D and L_L . For a fixed cross-sectional area of the detection section, zone length, assay time and SNR are all proportional to $A_L L_L$. Therefore in Figure 3, the contours of constant zone length, assay time and SNR, are the same except for a multiplicative constant. Unlike the case of fixed voltage, SNR for fixed current operation increases significantly by increasing the loading length. This is because zone length increases for large L_L , while the interface thickness remains unaffected by changing L_L . Thus, SNR (which is the ratio of zone length and characteristic interface thickness) increases by using longer L_L , for fixed current systems.

Further, by using Eqs. (15), (19) and (20) we note that,

$$\text{SNR} \propto \frac{T}{A_D^2}. \quad (22)$$

The relation above shows that for a fixed assay time, T , we can obtain very high SNR by decreasing A_D . We note that such behavior is not observed for fixed voltage operation, where higher SNR is accompanied by longer assay time.

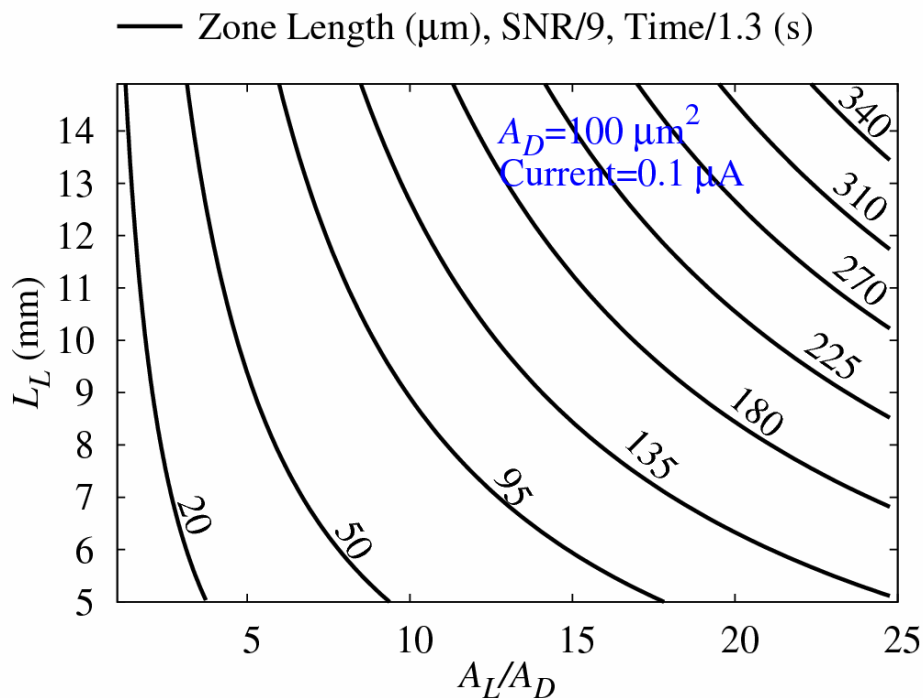


Figure 3: Variation of zone length, SNR and assay time with cross-sectional area ratio (A_L / A_D) and loading length (L_L), for fixed current operation. Solid lines show the contours of constant zone length for varying cross-sectional area ratio and loading length. The contours of zone length are the same as those shown in Figure 1, as zone length is independent of the applied voltage or current. For a fixed cross-section of the detection section, variation of SNR and assay time with A_L and L_L is similar to that of the zone length. Therefore, the contours of SNR and detection time have the same shape as those of zone length, except for a multiplicative constant. As an example, $50 \mu\text{m}$ zone length is equivalent to SNR = 450 and assay time of 66 s. For these calculations we used a fixed current of $0.1 \mu\text{A}$ and a detection section with $100 \mu\text{m}^2$ cross-sectional area. ITP buffer chemistry for these calculations is the same as that used in Figure 1.

References

1. Bercovici, M., Lele, S.K., Santiago, J.G., *J. Chromatogr. A* 2009, 1216, 1008-1018.
2. Bercovici, M., Lele, S.K., Santiago, J.G., *J. Chromatogr. A* 2010, 1217, 588-599.
3. Zhukov, M., Yu, U.S.S.R. *Comput. Maths. Math. Phys.* 1984, 24, 138-149.
4. Alberty, R. A., *J. Am. Chem. Soc.* 1950, 72, 2361-2367.
5. Jovin, T. M., *Biochemistry* 1973, 12, 871-879.
6. Bahga, S.S., Bercovici, M., Santiago J.G., *Electrophoresis* 2010, 31, 910-919.
7. Khurana, T.K., Santiago, J.G., *Anal. Chem.* 2008, 80, 6300-6307.
8. Saville, D.A., Palusinski, O.A., *AIChE J.* 1986, 32, 207.